

THERMAL CREEP BEHAVIOUR OF ZIRCALOY-4 CLADDING TUBES

Young Suk Kim

Korea Atomic Energy Research Institute, P.O. Box 7, Daejeon, 305-606, Korea

ABSTRACT

As it was found that the steady state creep rate and the primary creep strain of Zircaloy-4 cladding tube increase with the increasing amount of cold working at the final pilger pass, the generalized creep model has been derived which can account for the effect of the amount of cold working on the creep of Zircaloy-4 cladding tube :

$$\epsilon_t = 6.027 \cdot 10^{-3} \cdot RA \cdot \sigma_{eff} (1 - \exp(-34.13 \cdot \epsilon_s \cdot \sqrt{t})) + \epsilon_s \cdot t,$$

where ϵ_t = total thermal creep strain, ϵ_s = the steady state creep rate = $RA^2/(1-RA^2) \cdot 9.477 \cdot 10^{15} \cdot \exp(-30084/T(^{\circ}K)) \cdot \exp(3300 \cdot \sigma_{eff}/E)$, E = elastic modulus, σ_{eff} = effective stress, t = time, and RA = the reduction of area at the final pilger pass.

1. Introduction

The creep behavior of Zircaloy-4 material has been extensively studied because its understanding is essential in reliably predicting fuel rod performance. To date, however, most studies on deformation of Zircaloy-4 material have focused on the effect of heat treatments, textures and compositions [1,2], not on the detailed microstructural features such as the amount of cold working. As thermal creep of Zircaloy-4 material would be controlled by the motion of dislocation, more attention should have to be paid to the effect of the amount of cold working that the tube may experience during the pilgering process.

The purpose of this study is to investigate thermal creep behavior of four different Zircaloy-4 tubes with various amounts of cold working at the final pilger pass, and moreover to derive a generalized thermal creep model which can cover the effect of the amount of cold working on the creep behavior. To single out the effect of cold working, Zircaloy-4 tubes with the almost identical texture and mechanical properties were used. This generalized model will facilitate to optimize the tube reduction schedules which simultaneously can meet the requirements associated with high creep strength and radial texture.

2. Experimental details

2.1. Materials

In order to see the effect of the amount of cold working on the creep behavior, four different kinds of Zircaloy-4 tubes were used for long term creep tests, which were referred herein to as Tubes A, B, C and D. Table 1 shows the mechanical and microstructural features of Tubes A, B, C and D, respectively. It is worth noting that Tubes B, C and D have almost the same Yield Strength at room temperature. As only Tube A has undergone the stress

relieved heat-treatment, Tubes A has exhibited higher Yield Strength than the others. The amount of cold working of Tubes A, B, C and D at the final pilger pass was 81.7, 80.3, 74.7 and 64.3 %, respectively in terms of the reduction of area(RA). Due to different tube dimensions as shown in Table 1, Tubes B and C have experienced the same manufacturing procedures but the final pilger pass so that all the related properties are identical though the radial texture of Tube C was a bit higher than that of Tube B. But the amount of cold working at the final pilger pass between each other, in this case, was not much different. However, in case of Tubes B and D, the amount of cold working of Tube D at the final pilger pass differed much from that of Tube B even though tube properties including mechanical properties and microstructural features were found identical.

2.2. Creep testing

The creep tests were conducted by internal pressurization of eight inch long specimens. The temperature variation along the tube was ± 1 °C. Tube pressure was monitored by a transducer for the duration of the exposure. Tube dimensions were obtained by measuring the tube ID at each end with micrometer and the tube OD with a laser micrometer system. The accuracy of the laser measurement system was 0.000015 inch. The biaxial creep tests were conducted at temperatures of 350 °C and 400 °C and hoop stresses of 80 and 150 N/mm².

3. Results and Discussion

3.1. Thermal creep behavior of Tubes A through D

The creep tests were performed for up to 2650 h on 4 different cladding tubes, Tubes A through D, which underwent different amount of cold working at the final pilger pass. Figs. 1 and 2 exhibit thermal creep behavior of Tubes A through D under 2 kinds of hoop stresses at 400 °C, and Fig. 3 exhibits thermal creep behavior at 350 °C and 150 N/mm². Here, the creep strain represents the mid-wall OD strain. All the creep results shown in Figs. 1 to 3 indicated that the steady state creep rate and creep strain are strongly related to the amount of cold working expressed in the reduction of area. That is, Tube D with 64.3 % RA at the final pilger pass exhibits the higher creep strength while Tube A with 81.7 % RA turns out to have lower creep strength and higher creep strain. Among other things, comparison of the creep behavior of Tubes B and C provides the clear evidence that the higher the amount of cold working(= the reduction of area), the higher the steady state creep rate. It is to note that all the manufacturing processes but the last pilger pass of both Tube B and Tube C are almost the same, resulting in the same mechanical properties except for the texture parameter. On top of that, the steady state creep rate of Tube A with 81.7 % RA is almost comparable to Tube B with 80.3 % RA. Considering that Tube A was stress relieved during the final heat treatment and Tube B was partially recrystallized to get the degree of recrystallization of 10 to 24 %, the above result also explains that the steady state creep rate is determined predominantly by the amount of cold working at the final pilger pass. Therefore, the most important parameter in determining creep strength of Zircaloy-4 cladding tubes must be the amount of cold working at the final pilger pass, not the degree of recrystallization.

Tube B was partially recrystallized and Tube A was stress relieved such that Tube B may have lower dislocation density. Therefore, the fact that the steady state creep rate for Tubes A and B was comparable indicates that the steady state creep rate proceeds independently of dislocation density. As the generalized creep model derived in the following equation (3) proves that the steady state creep rate is controlled by dislocation climb, the steady state creep rate may be controlled by the rate at which edge dislocations or jogged screw dislocations climb. As it is well known that the concentration of point defects such as vacancies or interstitials increases with plastic deformation, higher amount of cold working at the final pilger pass may contribute to the generation of higher concentration of vacancies, leading to the increase in the creep rate.

3.2. Phenomenological thermal creep model

3.2.1. Steady state creep

To derive the steady state creep rate based on the creep data shown in Figs. 1 to 3, Dorn's quasi-theoretical approach was employed for thermal creep equation in terms of the effective stress and mid-wall tangential strain on account of the experimental condition of relatively higher applied stresses and low temperature /3/:

$$\epsilon_s = C_1 \cdot D \cdot \exp(C_2 \cdot \sigma_{\text{eff}}/E) \quad \text{for } \sigma_{\text{eff}} > 10^{-3} E, \quad (1)$$

where ϵ_s = the steady state thermal creep rate at the mid-wall (% / day), σ_{eff} = the effective stress (N / mm²) = $1 / \sqrt{2} \cdot [(\sigma_t - \sigma_r)^2 + (\sigma_r - \sigma_{\text{ax}})^2 + (\sigma_{\text{ax}} - \sigma_t)^2]^{1/2}$, D = diffusion coefficient = $D_0 \cdot \exp(-Q/RT)$, Q = activation energy, R = gas constant, C_1, C_2 = constants, E = elastic modulus (N/mm²), and $\sigma_t, \sigma_{\text{ax}}, \sigma_r$ = tangential, axial and radial stresses.

Among other things, the specific steady state thermal creep rate was determined mainly based on the mid-wall creep rate of Tube B. Log-log plot of the mid-wall creep rate vs. σ_{eff}/E under constant temperature, as shown in Fig. 4, resolved the constant C_2 to be 3300. In addition, the activation energy of Q/R was determined from the relationship of the creep rate of Tube B vs. temperature under constant stress condition. Thus, the steady state creep rate which can be applicable only to Tube B is represented as follows:

$$\epsilon_s = 1.72 \cdot 10^{16} \cdot \exp(-30084/T(^{\circ}\text{K})) \cdot \exp(3300 \cdot \sigma_{\text{eff}}/E). \quad (2)$$

As Figs. 1 to 3 indicate that the steady state creep rate must be a function of the amount of cold working at the final pilger pass, that is the reduction of area (RA), the above creep equation was generalized by putting the following parameter of $RA^2/(1-RA^2)$ into the equation (2). Therefore, the generalized equation can be described as

$$\epsilon_s = RA^2/(1-RA^2) \cdot 9.477 \cdot 10^{15} \cdot \exp(-30084/T(^{\circ}\text{K})) \cdot \exp(3300 \cdot \sigma_{\text{eff}}/E). \quad (3)$$

Comparison of the measured creep rate and the predicted one by the above generalized creep equation (3), as shown in Fig. 5, proves that the generalized thermal creep model is quite valid and can cover the effect of the amount of cold working at the final pilger pass.

The generalized creep equation shown in the equation (3) exhibits the apparent activation energy of 251 KJ/mole which is quite in excellent agreement with the activation energy of 252 KJ/mole by K. L. Murty /3/ and of 260.4 KJ/mole by Lyashenko /4/. Note that Holmes proposed as the activation energy of 245.7 KJ/mole is comparable to that for zirconium diffusion in Zr-Sn alloys that the dislocation climb mechanism is the major controlling step /5/. Therefore, the activation energy derived from the generalized thermal creep model suggests that thermal creep is controlled by dislocation climb even though the test temperature is around half of the alpha-beta transition temperature, not half of the melting temperature. This finding is consistent with the results shown in Figs. 1 to 3 that the creep rates and strains increase with the amount of cold working at the final pilger pass. In other words, if thermal creep is controlled by dislocation climb, lower amount of cold working brings on the lower concentration of vacancies generated, leading to retarding the rate at which edge dislocations or jogged screw dislocations climb, which eventually lowers the steady state creep rate. As a result of that, if lower thermal creep rate of the Zircaloy-4 tube would be desirable from the view point of the fuel rod design, it would be better to keep the reduction of area at the final pilger pass as low as possible.

3.2.2. The primary creep

Based on the creep data obtained shown in Figs. 2 and 3, the primary creep was assumed to decrease with exponential dependence of the square root of time :

$$\epsilon_p = \epsilon_p^{\circ} \cdot (1 - \exp(-C_3 \cdot \epsilon_s \cdot \sqrt{t})), \quad (4)$$

where ϵ_p = the primary creep strain (%), ϵ_p° = the primary creep constant (%), ϵ_s = the steady state creep rate shown in the equation (3), t = time, and C_3 = a constant.

The primary creep constant, ϵ_p° , was determined from Figs. 1 to 3 by extrapolating the secondary creep rate to zero time to intercept the Y-axis of the plot of the mid-wall creep strain vs time. As it was found that the thermal creep model was closely related to the amount of cold working as well as the applied effective stress, the primary creep constant can be correlated with the effective stress applied and the amount of cold working:

$$\epsilon_p^\circ = C_4 \cdot \sigma_{\text{eff}} \cdot RA, \quad (5)$$

where C_4 = a constant, and RA = the amount of cold working in terms of the reduction of area (%/100). By making use of the creep data obtained at the conditions of either 350 °C/150 MPa or 400 °C/80 MPa in which the change in the primary thermal creep behavior with time can be seen clearly, the constant C_3 and C_4 were determined to be 34.13 and 6.027×10^{-3} , respectively.

3.2.3 Comparison of the predicted and the measured creep strain

Total thermal creep can be derived by combining the primary creep and the secondary creep as shown in the equation (6):

$$\epsilon_t = 6.027 \cdot 10^{-3} \cdot RA \cdot \sigma_{\text{eff}} \cdot (1 - \exp(-34.13 \cdot \epsilon_s \cdot \sqrt{t})) + \epsilon_s \cdot t, \quad (6)$$

where ϵ_t = total thermal creep strain (%), ϵ_s = the steady state creep rate = $RA^2/(1-RA^2) \cdot 9.477 \cdot 10^{15} \cdot \exp(-30084/T(^{\circ}\text{K})) \cdot \exp(3300 \cdot \sigma_{\text{eff}}/E)$, E = elastic modulus (N/mm^2), σ_{eff} = effective stress (N/mm^2), and t = time in day.

Fig. 6 displays the comparison of the measured total creep strain and the calculated one for four different kinds of Zircaloy-4 Tubes at various conditions. Irrespective of the type of Zircaloy-4 Tubes, very excellent agreement was observed for all the conditions.

4. Conclusion

Based on thermal creep behavior of Zircaloy-4 cladding tubes that the steady state creep rate and the primary creep strain increase with the reduction of area at the final pilger pass, the generalized creep model which can account for the effect of the amount of cold working on the creep was derived as follows:

$$\epsilon_t = 6.027 \cdot 10^{-3} \cdot RA \cdot \sigma_{\text{eff}} \cdot (1 - \exp(-34.13 \cdot \epsilon_s \cdot \sqrt{t})) + \epsilon_s \cdot t,$$

where ϵ_t = total thermal creep strain (%), ϵ_s = the steady state creep rate = $RA^2/(1-RA^2) \cdot 9.477 \cdot 10^{15} \cdot \exp(-30084/T(^{\circ}\text{K})) \cdot \exp(3300 \cdot \sigma_{\text{eff}}/E)$, E = elastic modulus (N/mm^2), σ_{eff} = effective stress (N/mm^2), t = time in day, and RA = the reduction of area at the final pilger pass (%). It is proposed that the reason why the steady state creep rate increases with the amount of cold working at the final pilger pass may be attributed to higher concentration of vacancies necessary for edge or jogged screw dislocations to climb. The activation energy of 251 KJ/mole was obtained from the generalized thermal creep model also confirming that dislocation climb is the major controlling step. The generalized creep model was verified to be able to predict thermal creep of Zircaloy-4 cladding tubes which undergo various pilger passes.

References

- /1/. Kallstrom, K., Andersson, T., and Hofvenstam, A. (1974), ASTM STP, 551, 160.
- /2/. Filderis, V. (1975), Atomic Energy Rev., 13, 51.

- /3/. Murty, K.L., Clevinger, G.S. and Papazoglou, T.P. (1977), Trans. of the 4th Int'l Conf. on Structural Mechanics in Reactor Technology, vol. C3/4, San Francisco, CA.
- /4/. Lyashenko, V.S., Bykor, V.N., and Pavlinov, L.V. (1960), Phys. Metals Metallography, vol. 8.
- /5/. Holmes, J.J. (1964), J. Nucl. Mater., vol. 13, 137

Table 1. Characterization of the Zircaloy-4 Cladding Tubes.

Item	Tube A	Tube B	Tube C	Tube D
1. Dimension (OD x W) (mm)	9.5 x 0.58	9.5 x 0.64	10.75 x 0.73	9.5 x 0.64
2. Reduction of Area at the Final Pass (%)	81.7	80.3	74.7	64.3
3. Heat Treatment	SR*	PR**	PR	PR
4. Degree of Recrystallization (%)	-	13-24	13-24	10-24
5. Texture Parameter (fr)	-	0.52	0.56	0.52
6. Yield Strength at RT (N/mm ²)	652	507	493-517	>471
7. Tensile Strength at RT (N/mm ²)	849	709	681-705	>664
8. Elongation (%)	-	19-20	21.5-23.5	22

* : Stress Relieved,

** : Partially Recrystallized

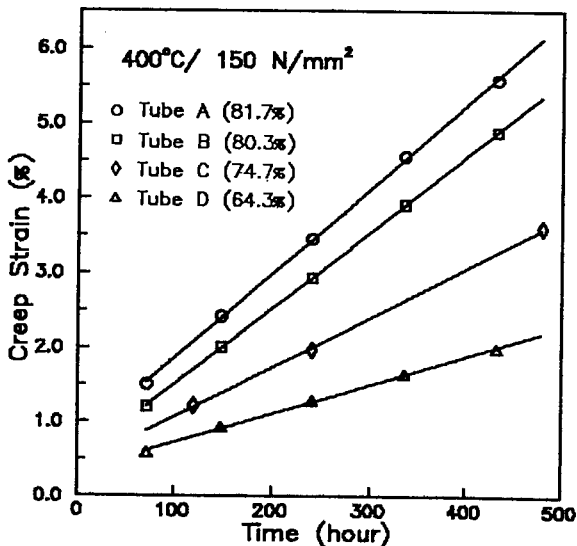


Fig. 1. Thermal Creep of Zircaloy-4 Tubes with Various Amount of Cold Working at the Final Pilger Pass at 400 °C and 150 N/mm²

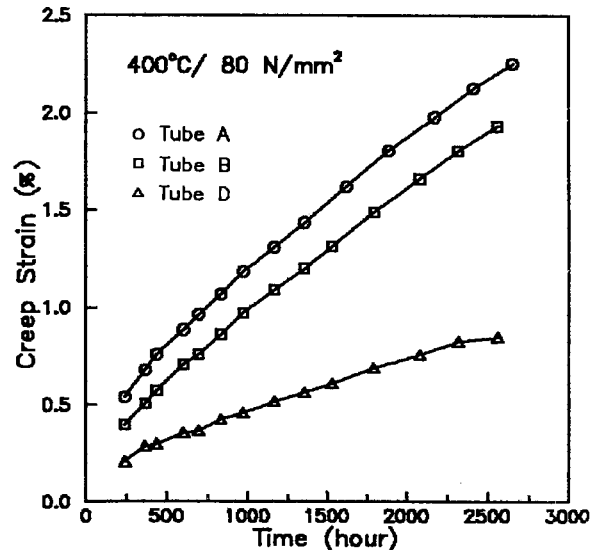


Fig. 2. Thermal Creep of Zircaloy-4 Tubes with Various Amount of Cold Working at the Final Pilger Pass at 400 °C and 80 N/mm²

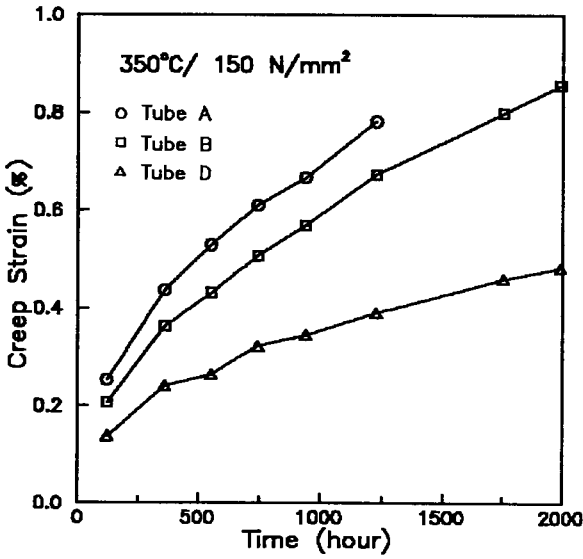


Fig. 3. Thermal Creep of Zircaloy-4 Tubes with Various Amount of Cold Working at the Final Pilger Pass at 350 °C and 150 N/mm²

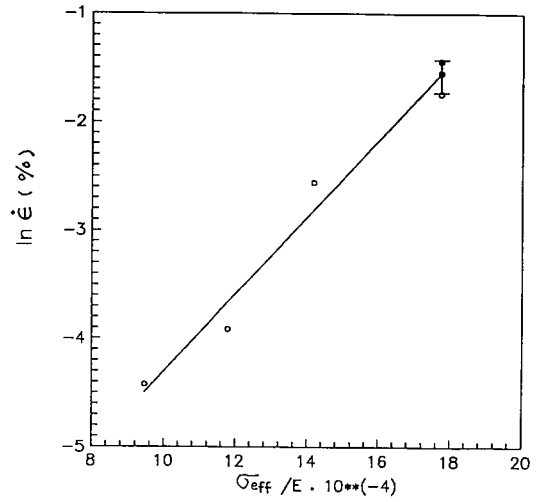


Fig. 4. The log-log Plot of the Mid-wall Creep Rate vs. σ_{eff}/E

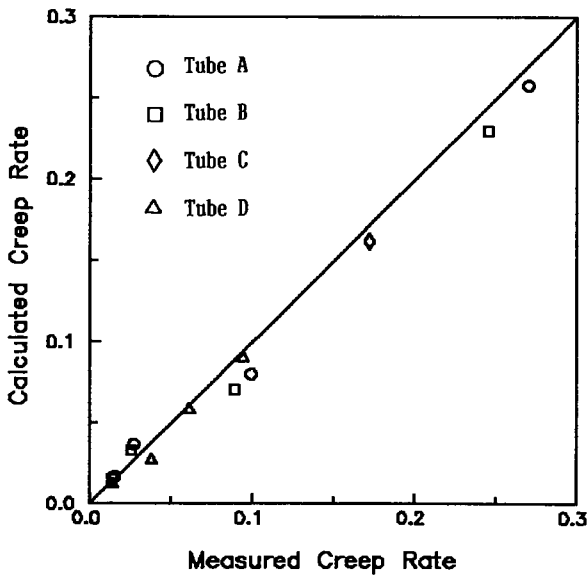


Fig. 5. Comparison of the Measured Steady State Creep Rate and the Calculated

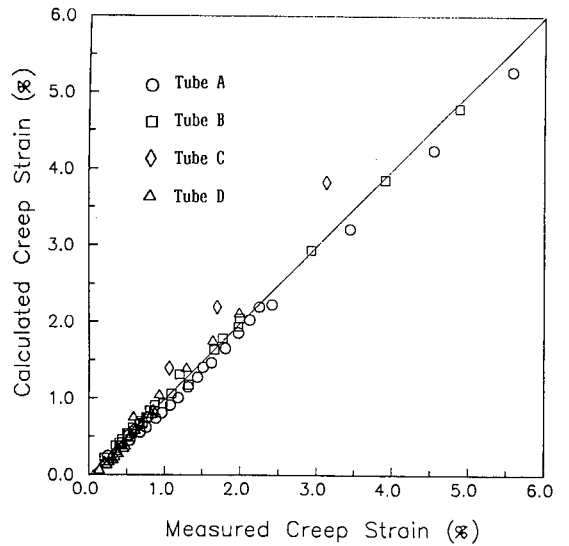


Fig. 6. Comparison of the Measured Creep Strains and the Calculated Ones by the Generalized Thermal Creep Model for 4 Different Tubes